

Surface layer temperature inversion in the Bay of Bengal: Main characteristics and related mechanisms

Pankajakshan Thadathil^{1*}, I. Suresh², S. Gautham², S. Prasanna Kumar²,
Matthieu Lengaigne³, R.R.Rao⁴, S. Neetu² and Akshay Hegde²

¹CSIR-National Institute of Oceanography, Regional centre, Cochin, India

²CSIR-National Institute of Oceanography, Goa, India

³Indo-French Cell for Water Sciences, IISc-NIO-IITM-IRD Joint International Laboratory,
NIO, Goa, India

⁴Indian Institute of Tropical Meteorology, Pune, India

*Corresponding author:

PankajakshanThadathil (email: pankaj@nio.org)
CSIR-National Institute of Oceanography
Regional centre, Cochin, India

Key Points:

1. Surface layer temperature inversion (SLTI) in the Bay of Bengal occurs during winter.
2. SLTI has significant interannual and intraseasonal variability.
3. Net surface heat loss is the most dominant process controlling the formation and maintenance of SLTI.

Abstract

Surface Layer Temperature Inversion (SLTI), a warm layer sandwiched between surface and subsurface colder waters, have been reported to frequently occur in conjunction with barrier layers in the Bay of Bengal (BoB), with potentially commensurable impacts on climate and post-monsoon tropical cyclones. Lack of systematic measurements from the BoB in the past prevented a thorough investigation of the SLTI spatio-temporal variability, their formation mechanisms and their contribution to the surface temperature variations. The present study benefits from the recent Research Moored Array for African-Asian-Australian Monsoon Analysis and Prediction (RAMA) buoys located in BoB along 90°E at 4°N, 8°N, 12°N, and 15°N over the 2006-2014 period. Analysis of data from these RAMA buoys indicates that SLTI forms after the summer monsoon, and becomes fully developed during winter (December – February). SLTI exhibits a strong geographical dependency, with more frequent (80% times during winter) and intense inversions (amplitude, $\Delta T \sim 0.7^\circ\text{C}$) occurring only in the northern BoB compared to central and southern Bay. SLTI also exhibits large interannual and intraseasonal variations, with intraseasonal amplitude significantly larger ($\Delta T \sim 0.44^\circ\text{C}$) than the interannual amplitude ($\sim 0.26^\circ\text{C}$). Heat budget analysis of the mixed layer reveals that the net surface heat loss is the most dominant process controlling the formation and maintenance of SLTI. However, there are instances of episodic advection of cold, low-saline waters over warm-saline waters leading to the formation of SLTI as in 2012-2013. Vertical processes contribute significantly to the mixed layer heat budget during winter, by warming the surface layer through entrainment and vertical diffusion.

1. Introduction

The Bay of Bengal (hereafter, BoB), a tropical semi-enclosed basin strongly influenced by the Indian monsoons, is characterized by large seasonal freshwater influx from rivers as well as excess precipitation over evaporation [Shenoi *et al.*, 2002]. A large fraction of the net freshwater flux into the ocean occurs during the summer monsoon and the early post-monsoon seasons, with near-equal contributions from continental runoffs (dominated by two major river systems, namely, the Ganges-Brahmaputra and the Irrawaddy) and monsoonal rainfall [Chaitanya *et al.*, 2014]. These freshwater sources are predominantly located in the northern BoB, making the sea surface salinity (SSS) there as low as ~28 psu just after the summer monsoon [Rao and Sivakumar, 2003; Akhil *et al.*, 2014]. The diluting effect of the rainfall and the river runoff is confined primarily to the upper ocean layers, resulting in sharp near-surface salinity stratification [Rao and Sivakumar, 2003; Thadathil *et al.*, 2007; Girishkumar *et al.*, 2011].

This strong near-surface salinity stratification increases the vertical stability of the upper ocean layer and helps to maintain a thin mixed layer [Mignot *et al.*, 2007; Thadathil *et al.*, 2007; Girishkumar *et al.*, 2013; Maes and O’Kane, 2014]. The salinity stratification often leads to the formation of barrier layer [Lukas and Lindstrom, 1991], an isothermal salinity-stratified layer located below the mixed layer. Barrier layers in BoB develop during fall (October – November) and peak during winter (December – March) [Rao and Sivakumar, 2003; de Boyer Montégut *et al.*, 2007]. They prevent turbulent entrainment of cooler thermocline water into the mixed layer and consequently maintain a warm sea surface temperature (SST) after the southwest monsoon [Shenoi *et al.*, 2002; de Boyer Montégut *et al.*, 2007] and thus reduce the negative oceanic feedback on the post-monsoon tropical cyclones [eg: Neetu *et al.*, 2012], favouring their intensification.

Barrier layers have regularly been reported to occur in conjunction with inversions in the vertical temperature profiles [Thadathil and Gosh, 1992; Thadathil *et al.*, 2002; Shankar *et al.*, 2004; Thompson *et al.*, 2006; Girishkumar *et al.*, 2013; Drushka *et al.*, 2014], in which temperature increases with depth due to the presence of a warm subsurface layer (inversion layer) sandwiched between surface and subsurface colder waters. Figure 1c illustrates one such occurrence of temperature inversion lasting from January to March 2013, as recorded by an Argo float (Figure 1a) from the northern part of the BoB. The beginning of 2013 (Figure 1d) was, indeed, characterized by a strong surface freshening (salinity ~30 psu) associated with a very sharp salinity stratification (a salinity difference of ~4 psu in the top 100-m depth), accommodating an inversion layer of 60-m thickness with temperatures ~3°C higher than that at the surface layer (Figure 1c). Although persisting through February-March, the amplitude of this surface freshening and the associated temperature inversion

weakened from late January onwards. Such a warm-water layer will, hereafter, be referred to as the Surface Layer Temperature Inversion (SLTI) (Figure 1b) throughout the text. In the presence of fresh surface waters and a barrier layer underneath, SLTI can occur when warming within the barrier layer is greater than the warming of the surface layer [Girishkumar *et al.*, 2013]. Given that the density stratification remains statically stable, the increased stability of the water column induced by the salinity stratification can thus accommodate the formation of SLTI by compensating the stability loss due to increase in the temperature with depth. Warming of the subsurface waters within the barrier layer usually arises from the shallow mixed layer that allows increased penetration of shortwave radiation at its base [Kurian and Vinayachandran, 2006; Mignot *et al.*, 2012]. On the other hand, SLTI can also occur due to cooling of mixed layer caused by net surface heat loss through increased latent heat flux, decreased surface shortwave radiation and/or increased shortwave penetration, and also by horizontal advection process [Girishkumar *et al.*, 2013].

Analysis of historical data [Thadathil *et al.*, 2002] and measurements from ARGO floats [Thompson *et al.*, 2006; Thadathil *et al.*, 2007] revealed large spatio-temporal variations of SLTI over BoB, with spatially organised SLTI occurring mainly along the coastal regions of the western and north-eastern parts of the Bay during winter, when barrier layers are most prominent. An investigation of SLTI variability has long been limited to the seasonal timescale due to paucity of long-term temperature and salinity measurements at high temporal resolution. Using repeated XBT data in the northern BoB, Thadathil *et al.* [2002], however, reported significant SLTI interannual variability and attributed it to the year-to-year variations in freshwater forcing. The availability of time-series observations of physical (temperature, salinity and current) and surface meteorological parameters from Research Moored Array for African-Asian-Australian Monsoon Analysis and Prediction (RAMA) buoys in the BoB (Figure 1a) now allows a more accurate description of the intraseasonal to interannual variability of SLTI. Girishkumar *et al.* [2013] analysed the data from one such mooring located in the central part of the Bay (8°N, 90°E) and reported large intraseasonal and year-to-year (two winters during 2006-2008) variations in the frequency and magnitude of temperature inversions. However, the buoy considered in their study is not located within the core region of the intense and most frequent inversions, which usually is most prominent in the north-eastern part of the Bay [Thadathil *et al.*, 2002].

In this study, we provide a more comprehensive description of SLTI by analysing the data from all four available RAMA buoys in BoB (Figure 1a), extending from 8°N to 15°N and for a longer period (seven winters during 2007-2014), and investigate the mechanisms driving the SLTI variability. The paper is organized as follows. Data and method are provided in section 2. A description of the main characteristics of SLTI and its spatio-temporal variability are presented in Section 3. Section 4 discusses the mechanisms driving the SLTI variability observed at the northernmost buoy (15°N, 90°E) that exhibits the largest and most frequent SLTI. Section 5 discusses the contribution of SLTI

to mixed layer heat budget through vertical processes. Lastly, main findings of the present study are summarized in Section 6.

2. Data and Method

2.1. SLTI characteristics derived from RAMA temperature and salinity profiles

Data from the four RAMA buoys (Figure 1a) located in the BoB along 90°E at 4°N (2006-2013), 8°N (2006-2013), 12°N (2007-2014), and 15°N (2007-2014) are analysed to describe and understand the occurrence of SLTI in the Bay. These buoys provide daily time series of temperature collected at 1, 10, 13, 20, 40, 60, 80, 100, 120, 140, 180, 300, and 500-m depths and of salinity collected at 1, 10, 20, 40, 60, and 100-m depths. The vertical profiles from these buoys are linearly interpolated onto a common 1-m vertical-grid resolution.

Following *Monterey and Levitus* [1997], a fixed density criterion, i.e., a change in density from the ocean surface of 0.125 (sigma units), is used for calculating the mixed layer depth (MLD). The isothermal layer depth (ILD), the depth of the top of thermocline, is defined to be the depth at which the temperature decreases by 1°C from the SST. This ILD definition is consistent with that of MLD, resulting in similar values when the salinity stratification is vertically homogeneous. Barrier Layer Thickness (BLT) is defined as the difference between ILD and MLD. Following *Girishkumar et al.* [2013], we identify inversion in the vertical temperature profile when the temperature at a depth is greater than SST by 0.1°C, a threshold that largely exceeds the accuracy of original RAMA temperature measurements ($\pm 0.02^\circ\text{C}$). We also derive the main characteristics of the SLTI from the depth profiles of temperature and salinity as illustrated in Figure 1b. The amplitude of the inversion (ΔT) is calculated as the difference between the maximum temperature (T_{max}) in SLTI and the SST. The amplitude of the salinity stratification (ΔS) during the period of inversion is defined as the difference between the salinity at the depth of maximum temperature in the SLTI and the SSS.

2.2. Mixed layer heat budget

As noted in the introduction, temperature inversions can occur due to cooling of the surface layer through heat loss, horizontal advection, or warming of the subsurface layer through shortwave penetration below the mixed layer. These plausible causes are examined by performing a heat budget analysis of mixed layer, using the expression (see for e.g., *Rao and Sivakumar* [2000]) given below:

$$\frac{\partial T}{\partial t} = \frac{Q_{\text{net}} - Q_{\text{pen}}}{\rho C_p h} - \left[u \frac{\partial T}{\partial x} + v \frac{\partial T}{\partial y} \right] + \text{Residual} \quad (1)$$

where $\frac{\partial T}{\partial t}$ is the mixed layer temperature tendency, the first term on the RHS represents the heat fluxes due to atmospheric forcing, in which Q_{net} is the net surface heat flux, Q_{pen} is the penetrative shortwave below the mixed layer, $\rho (= 1023 \text{ kg/m}^3)$ is the density of seawater, $C_p (= 3989.2 \text{ J/kg/K})$ is the specific

heat capacity of seawater, and h is the MLD. The terms $-u \frac{\partial T}{\partial x}$ and $-v \frac{\partial T}{\partial y}$ are the zonal and meridional components of horizontal advection respectively. The difference of the atmospheric forcing plus the horizontal advection terms from the mixed layer temperature tendency term is the “Residual”. In the absence of measurement errors, the residual mainly accounts for the vertical processes (entrainment and vertical diffusion), the contribution from horizontal diffusion being almost negligible [Halkides *et al.*, 2011]. However, in our analysis, the residual will include errors in the buoy measurements.

In equation (1), we use the daily MLD computed from the buoy density profile as detailed in Section 2.1. Q_{net} is obtained as the sum of latent heat flux (Q_{lat}), sensible heat flux (Q_{sen}), surface shortwave radiation (Q_{short}) and long wave radiation (Q_{long}). Q_{lat} , Q_{long} and Q_{sen} are estimated using the Coupled Ocean Atmosphere Response Experiment (COARE) bulk flux algorithm [Fairall *et al.*, 2003] using the air temperature, SST, relative humidity and wind speed from the RAMA buoy. Q_{short} is derived from downwelling shortwave flux measured by the buoy and corrected for albedo at the sea surface (downwelling shortwave radiation is multiplied by 0.945). Whenever the buoy data is not available, the data from TropFlux [Praveen Kumar *et al.*, 2011] is used. Q_{pen} is estimated as:

$$Q_{\text{pen}} = 0.47Q_{\text{short}}[V_1 e^{-\frac{h}{\zeta_1}} + V_2 e^{-\frac{h}{\zeta_2}}]$$

Where ζ_1 and ζ_2 are the attenuation depths of long visible, short visible and ultraviolet wavelengths, and h is the MLD in meters [Morel and Antoine, 1994; Sweeney *et al.*, 2005]. As in Girishkumar *et al.*, [2013], the values of V_1 and V_2 , ζ_1 and ζ_2 are estimated from MODIS 8-day composite chlorophyll-a (mg m^{-3}) data using the method of Morel and Antoine [1994]. The approximate values of these parameters are 0.39, 0.69, 1.52, and 18.9 respectively.

As the temperature is relatively uniform from the surface to the base of the mixed layer, we calculate the horizontal advection terms using the SST derived from the optimally interpolated microwave plus infrared SST product at 9-km resolution. Horizontal temperature gradient is estimated as the forward difference of ~ 25 -km averaged SSTs on either side of buoy location. Zonal (u) and meridional (v) currents are derived from the 10-m current measurements at the RAMA buoys. Surface currents shown on Figure 11 are derived from the Ocean Surface Current Analysis (OSCAR), a satellite-based estimate of 0–30m averaged currents on a $1/3^\circ$ Mercator [Bonjean and Lagerloef, 2002].

3. SLTI main characteristics

Daily evolution of vertical temperature (left panel) and salinity (right panel) from October 2012 to May 2013 are shown in Figure 2 for the four RAMA buoys considered in this study. The dashed and continuous black lines represent MLD and ILD, respectively. The dots indicate the presence of temperature inversion and are placed at the centre of the SLTI, with their colors representing the magnitude of ΔT . SLTIs are present at all four buoy locations, but exhibit a strong geographical

dependency in their intensity and the frequency of their occurrence. The northern-most buoy at 15°N displays a far stronger salinity stratification, with ΔS exceeding 3 psu, and considerably larger ΔT exceeding 2°C compared to the other three southern buoys (at 12°N, 8°N, and 4°N), which exhibit a rather weak salinity stratification (up to 1.5 psu) and ΔT that rarely exceeds 1°C.

Figure 3 shows the climatological characteristics (viz., the percentage of occurrence of inversion, ΔT amplitude and inversion layer thickness (LT)) of the SLTI for all four buoys to assess if the aforementioned geographical dependency of the SLTI characteristics holds true over the entire period for which the data is available. SLTI occurs (at their peak, December – February) only ~15% of the times at the southern part of the Bay (Figure 3d), and are very weak (~0.25°C) with LT ~40 m. In the central part of the Bay (Figures 3b and 3c), the percentage of occurrence (~30%) and the layer thickness (40-50m) of SLTI are slightly larger, but the amplitude of ΔT yet remains fairly weak (~0.25°C). This is in stark contrast with SLTI characteristics in the northern part of the Bay (Figure 3a). At this location, the SLTI exhibits a very strong seasonal cycle, with very frequent (~80%), thick (~60m) and intense (~0.7°C) SLTI from December to February as compared to October and March (~30%, ~30 m and ~0.3°C respectively). Consistent with *Thadathil et al.* [2002], the above analysis thus illustrates the strong geographical dependency of the SLTI seasonal characteristics, with frequent, intense and thick SLTI occurring only in the northern part of the Bay during winter. Therefore the SLTIs over the northern BoB are likely to have stronger impact on the oceanic heat budget compared to those in the southern BoB. Henceforth, we will focus on analysis of the data from the northernmost buoy (at 15°N).

Figure 4 provides panels similar to those in Figure 2, but for the seven winters during 2007-2014 at the northernmost RAMA mooring. Although the seasonal SLTI variations discussed above are evident in this figure, with more prominent SLTI during winters, it also depicts considerable intraseasonal to interannual variations in the SLTI. For instance, strong intraseasonal oscillations are evident during winter 2012-2013, in particular, at the beginning and at the end of January 2013, with ΔT values exceeding 2°C and also during early February 2013, with ΔT exceeding 1°C. The period 2012-2013 also displays the most persistent occurrence of SLTI, which is seen over two months period from the first week of January to the first week of March 2013. In contrast, the winters of 2007-2008 and 2010-2011 exhibit less persistent and weaker SLTI, with weak intraseasonal variations.

Figure 5 allows quantifying the respective contributions of intraseasonal and interannual variations to the total SLTI variability during winter. In this figure, SLTI characteristics (ΔT and LT) are shown for each winter from December to February during when persistent and intense SLTI occurs. The interannual component is defined as the mean value of the seasonal anomalies (seasonal cycle removed) during December – February for each year (red horizontal bars) and the intraseasonal

variations are computed as the deviation from the interannual component for each year. ΔT does not exhibit large interannual fluctuations, except in 2013 when ΔT reach $\sim 1.3^\circ\text{C}$ compared to 0.5°C - 0.7°C for the rest of the years. In contrast, strong intraseasonal fluctuations ($\pm 1^\circ\text{C}$) are evident on the top of the seasonal averages. Consequently, the ΔT amplitude at intraseasonal time scale is larger ($\sim 0.44^\circ\text{C}$) than that at interannual scale ($\sim 0.26^\circ\text{C}$). This contrast is even more striking for LT, whose variations ranges from 10 to 100 m, with a far larger contribution from intraseasonal (amplitude ~ 14 m) compared to the interannual component (~ 4 m).

The relationships between different SLTI characteristics are examined in Figure 6. Figure 6a, which shows scatter plot of LT vs. ILD, indicates that SLTI thickness is mainly controlled by the depth of the thermocline (correlation between LT and ILD is 0.87, which is significant at 95% confidence level) rather than the depth of the halocline in the surface layers (0.01 correlation between LT and MLD, not shown). In agreement with *Girishkumar et al.*, [2013], Figure 6b indicates a non-linear relationship between LT and ΔT ; thin SLTI (< 40 m) are systematically associated with weak temperature inversions ($\Delta T < 0.5^\circ\text{C}$), while ΔT increases considerably for thick SLTI (> 60 m). It must however be noted that weak to moderate ΔT ($< 1^\circ\text{C}$) can be observed even for large LT (60 to 80 m).

4. Driving processes

As noted in the introduction, SLTI can form only in the presence of strong upper ocean salinity stratification. Figure 7 presents the histogram of SSS normalized by the total number of observations (normalized distribution of SSS) for both inversion (when $\Delta T > 0.1^\circ\text{C}$) and non-inversion cases. This figure highlights that the strong surface freshening (SSS < 31 psu) is systematically related to the temperature inversions, while the moderate surface freshening ($31 \text{ psu} < \text{SSS} < 33 \text{ psu}$) can result in both inversion and non-inversion cases. This figure thus illustrates that, although the strong salinity stratification is a prerequisite for the SLTI formation, it is not a sufficient condition. Figures 8a and 8b further demonstrates that, once SLTI is formed, its amplitude is strongly related to the strength of the salinity stratification (correlation > 0.8) and to the surface freshening (correlation ~ -0.7). Increased (decreased) upper ocean salinity stratification and lower (higher) SSS lead to more (less) intense SLTI.

In the presence of strong upper ocean salinity stratification, SLTI can form due to surface layer cooling and/or by warming below the mixed layer. Figures 8c and 8d, which provide scatter plots of ΔT against SST and T_{max} anomalies, illustrate that ΔT is more tightly related to the SST fluctuations (correlation ~ 0.7) compared to the subsurface temperature (T_{max}) variations (correlation ~ 0.4). Therefore, in the presence of upper ocean salinity stratification, the surface cooling processes (i.e., the SST variability) are key drivers of the SLTI formation and maintenance.

We further investigate the processes responsible for the SST variability at the buoy location. As mixed layer temperature is a proxy for SST, we perform mixed layer heat budget analysis described in Section

2.2 to understand the SST variability. Figure 9 presents the result of this analysis for three particular years. It is evident from this figure that the occurrence of inversions generally coincide with SST cooling events. During the 2008-2009 and 2009-2010 winters, the atmospheric forcing mainly drives the SST cooling. For instance, the strong surface cooling occurring in late December 2008 is strongly related to atmospheric heat loss in the mixed layer, while it appears to be unrelated to horizontal advection process, which indicates a warming tendency. Similarly, the SST cooling tendency in January 2010 is strongly related to the fluctuations in the atmospheric forcing rather than the horizontal advective process. This is in contrast with the situation seen during winter 2012-2013, when the SST tendency appears to be very consistent with the horizontal advection term rather than the atmospheric forcing. The above analysis thus suggests that the relative contributions of horizontal advection and net surface heat flux to evolution of the mixed layer temperature (and hence SST) depend on the period considered.

Figures 10a, 10b, and 10c show the scatter plots of the SST tendency against each of the three terms involved in the heat budget analysis (i.e., atmospheric forcing, horizontal advection and residual) over the entire period and hence allow a more general assessment of the processes driving the SST variations. This analysis indicates that the atmospheric forcing exhibits large fluctuations (between -0.4 and 0.4 $^{\circ}\text{C day}^{-1}$) and is the dominant contributor to the total SST tendency during winters at this location (Figure 10a), as demonstrated by the high correlation (0.46) between them. In contrast, the horizontal advection term shows a weaker variability (between -0.15 and 0.15 $^{\circ}\text{C day}^{-1}$) and is not significantly correlated with the SST tendency. In line with the previous studies (e.g. *Roxy and Tanimoto*, [2007]; *Vialard et al.*, [2011]), this analysis confirms that the atmospheric forcing is, by and large, the main driver of the SST evolution at this location, though the horizontal advection can also play a role as in early 2013 (see Figure 9c). Figures 10d, 10e, and 10f allow us to investigate further the main component of the atmospheric heat flux responsible for these atmospheric fluctuations. Latent heat flux dominates the net heat flux variability (Figure 10d), showing the largest correlation (0.87) and regression (0.49) coefficients amongst the different components. Although the shortwave flux (Figure 10e) contributes significantly to the net flux variability (0.7 correlation and 0.47 regression), the relationship is stronger for the non-inversion (blue dots) cases than during the inversion cases (red dots). This is also true with the weak penetrative shortwave flux as shown in Figure 10f. Thus the above analysis suggests that the net heat flux variations primarily drive the SST variability in this region, and the occurrence of SLTI in the presence of strong salinity stratification.

Although the above statement holds true for most of the winters, it is not the case with winter 2012, when horizontal advection strongly influences the SST variability (Figure 9c). This peculiar role of horizontal advection is further detailed on Figure 11, which shows weekly maps of SST and SSS, superimposed with surface currents (Geostrophic + Ekman) from late December 2012 to late January

2013. The black line in the left panels shows demarcation between cold and warm waters. The black star in Figure 11 shows the position of RAMA buoy (15°N). The strong cooling tendency observed in early January 2013 at buoy location is indeed driven by horizontal advection of cold and fresh waters from the head Bay, resulting in cooling of surface water by about 3°C and freshening by ~2 psu during late January compared to late December. This demonstrates the important role of surface advection in SLTI formation during specific periods.

5. Role of vertical processes

In the previous section, we discussed the role of atmospheric forcing and lateral advection in driving the SST tendency. We now focus on the remainder term (see section 2.2), which includes both measurement errors as well as the contribution from the vertical processes (entrainment and vertical diffusion); the contribution from horizontal diffusion being almost negligible [*Halkides et al.*, 2011]. The remainder term in our analysis is far from being negligible (Figure 9) and is generally positive during December – February, especially when inversion occurs and is negative during non-inversion periods (from March onwards). This behaviour is very consistent with that expected from the vertical processes, which would tend to warm the surface layer from below in the presence of SLTI (inversion period) and to cool the surface layer in the absence of SLTI (non-inversion period, i.e., when subsurface waters are colder than the surface waters). The remainder term, however, does not show any systematic relationship with the SST tendency term (Figure 10c). If we assume that the errors in the heat budget analysis (arising from the uncertainties in the measurements and the approximations used in the heat budget calculation) are smaller than the amplitude of the vertical processes, this remainder term can then be regarded as representing the contribution from the vertical processes and hence can be used to provide a rough estimate of their contribution to the surface heat budget during the winter season. In the following, we assume that the remainder term simply represents the vertical processes and discuss their contributions to the SST variability.

Figure 12a provides scatter plot of amplitude of the remainder term during inversion period as a function of amplitude of the inversion (ΔT). As expected from the contribution of vertical processes, this term is generally positive in the presence of SLTI and there is a clear warming tendency with increasing ΔT (correlation between the remainder term and ΔT is ~0.5), further suggesting that the remainder term in our heat budget equation (1) represents the vertical processes to a large extent. However, there are instances of negative contribution of this remainder term (Figure 12a) as well, which are found mostly in the weak to modest SLTI ($\Delta T < 1^\circ\text{C}$), that cannot be explained by the vertical processes. These features are most probably due to the uncertainties in our heat budget calculation. Figure 12b further quantifies the amplitude of this remainder term for non-inversion periods and for inversion periods as a function of ΔT . If we assume that the errors in the heat budget analysis would

result in an erratic contribution to the SST tendency, this analysis can somewhat be interpreted as the contribution of SLTI to the mixed layer heat budget. Under this assumption, SLTI contributes from $0.05^{\circ}\text{C day}^{-1}$ (during weak inversion period with $0.1^{\circ}\text{C} < \Delta T < 1^{\circ}\text{C}$) to more than $0.15^{\circ}\text{C day}^{-1}$ (during strong inversion period, $\Delta T > 1.5^{\circ}\text{C}$) to the mixed layer heat budget, with an average of $0.12^{\circ}\text{C day}^{-1}$. The contribution of vertical processes during non-inversion period is generally negative and accounts for an average cooling tendency of $0.07^{\circ}\text{C day}^{-1}$ in the mixed layer heat budget. On an average, the contribution of vertical processes to mixed layer temperature budget between inversion and non-inversion periods is about $0.18^{\circ}\text{C day}^{-1}$, and can be as large as $0.23^{\circ}\text{C day}^{-1}$ when strongest SLTI occurs. As these inversions occur frequently during winter in the northern part of the BoB (80% of the times in December - February period; see Figure 3a) and their contribution is of the same order of magnitude as that of the atmospheric forcing, SLTI is a major contributor to the SST variability and strongly contributes to damp the effect of winter cooling in this region. Thus SLTI acts to “warm” the upper ocean layer during “winter cooling” in the northern BoB.

6. Summary and conclusion

Surface Layer Temperature Inversions, a warm layer sandwiched between surface and subsurface colder waters, have been reported to frequently occur in conjunction with barrier layer in the BoB [Thadathil *et al.*, 2002]. SLTI affects surface temperature by entrainment and vertical mixing of warm subsurface water into the mixed layer [de Boyer Montégut *et al.*, 2007], and have, therefore, been suggested to have a significant impact on surface temperature during winter, by damping the effect of winter [de Boyer Montégut *et al.*, 2007; Girishkumar *et al.*, 2013] in BoB. The lack of systematic temperature and salinity profiles from the BoB in the past prevented a thorough investigation of the SLTI spatio-temporal variability, their formation mechanisms and their contribution to the surface temperature variations. The objective of the present study is to address these issues by making use of vertical temperature and salinity measurements derived from four RAMA buoys distributed in the BoB along 90°E at 4°N , 8°N , 12°N , and 15°N over a period of seven years.

Analysis of data from these RAMA buoys indicates that SLTI forms after the summer monsoon, and becomes fully developed during winter (December – February). In agreement with Thadathil *et al.* [2002], more frequent and intense inversions occur in the northern BoB compared to central and southern Bay. SLTI exhibits large interannual and intraseasonal variations, with intraseasonal amplitude significantly larger than the interannual amplitude.

Our analysis indicates that, in the presence of strong upper ocean salinity stratification, surface cooling processes are key drivers of the SLTI, rather than subsurface warming. Further assessment of various processes using mixed layer heat budget analysis reveals that the net surface heat loss is, by and large, the most dominant mechanism in the formation and maintenance of SLTI during the seven winters

considered in the 2006-2014 period. Episodic advection of cold, low-saline waters over warm, saline waters leads to the formation of SLTI as in the case of winter 2012-2013. Though a direct estimation of vertical processes is beyond the scope of the present study, an indirect assessment of vertical processes (assuming errors in the measurements or approximations in heat budget analysis are negligible) through the remainder term indicates that they contribute significantly to the mixed layer heat budget during winter, by warming the surface layer through entrainment and vertical diffusion.

Frequent occurrence of SLTI in the northern BoB during winter can contribute to the warming of surface layer by as large as $0.2^{\circ}\text{C day}^{-1}$, which is much higher than the estimate of $0.02^{\circ}\text{C day}^{-1}$ based on modelling studies of *de Boyer Montégut et al.* [2007] and *Mignot et al.* [2012]. Such a discrepancy may arise due to large region considered in these modelling studies, or from underestimation of SLTI in ocean models or uncertainties in our heat budget calculation. Our estimate of such a large contribution of vertical processes to the SST is also considerably higher than the estimate of *Girishkumar et al.* [2013] ($0.01^{\circ}\text{C day}^{-1}$ during January – February 2008 in their analysis), who did focus their analysis on the southern RAMA buoy at 8°N . This difference could be due to the presence of more frequent and intense SLTIs at 15°N compared to the southern BoB, which is characterized by infrequent and very weak occurrence of SLTI as illustrated in Figure 3.

It should, however, be noted that the results of the present study, obtained by analysing the data from the northernmost buoy, cannot be generalized to entire BoB, as SLTI is known to exhibit large spatio-temporal variations. Studying the SLTI characteristics in the entire Bay, however, is not possible due to limitations of observation in terms of the spatial and temporal coverages (only four buoys as of now in BoB over 7-years period). The warming rate of mixed layer due to the presence of SLTI (a maximum of $\sim 0.2^{\circ}\text{C day}^{-1}$) is subject to uncertainties in the heat budget calculations related to measurements errors (mainly fluxes) and approximations in heat budget calculation (for e.g., horizontal advection term). These uncertainties get absorbed in to the remainder term (treated as vertical processes) and hence would be interpreted as the influence of SLTI on heat budget via vertical processes. These shortcomings call for a dedicated modelling approach, which would allow accurate evaluation of the terms in the heat budget equation and to ascertain the conclusions based on the observations.

Acknowledgements

Authors acknowledge the Director, CSIR-NIO and CSIR for the support. This research work has been supported by the Naval Research Board (NRB) through a grant-in-aid project. RAMA data are provided by the TAO project office of NOAA/PMEL. Microwave+IR OI SST data are produced by Remote Sensing Systems and sponsored by National Oceanographic Partnership Program (NOPP), the NASA Earth Science Physical Oceanography Program, and the NASA MEaSUREs DISCOVER Project. Data are available at www.remss.com. The altimeter products are produced by

SSALTO/DUACS and distributed by AVISO. The Argo data were collected and made freely available by the International Argo project and the national program (coordinated by the Indian National Centre for Ocean Information Services) that contributes to it. Argo is a pilot program of the Global Ocean Observing System. OSCAR data were provided by NOAA/NESDIS under the National Oceanographic Partnership Program. This is NIO contribution AAAA.

References

Akhil, V. P., F. Durand, M. Lengaigne, J. Vialard, M. G. Keerthi, V. V. Gopalakrishna, C. Deltel, F. P. And, and C. de B. Montégut (2014), A modeling study of the processes of surface salinity seasonal cycle in the Bay of Bengal, *J. Geophys. Res. Ocean.*, *119*(6), 3926–3947, doi:10.1002/2013JC009632.

Bonjean, F., and G. S. E. Lagerloef (2002), Diagnostic Model and Analysis of the Surface Currents in the Tropical Pacific Ocean, *J. Phys. Oceanogr.*, *32*(10), 2938–2954, doi:10.1175/1520-0485(2002)032<2938:DMAAOT>2.0.CO;2.

De Boyer Montégut, C., J. Mignot, A. Lazar, and S. Cravatte (2007), Control of salinity on the mixed layer depth in the world ocean: 1. General description, *J. Geophys. Res. Ocean.*, *112*(C6), C06011, doi:10.1029/2006JC003953.

Chaitanya, a. V. S., M. Lengaigne, J. Vialard, V. V. Gopalakrishna, F. Durand, C. Kranthikumar, S. Amritash, V. Suneel, F. Papa, and M. Ravichandran (2014), Salinity Measurements Collected by Fishermen Reveal a “River in the Sea” Flowing Along the Eastern Coast of India, *Bull. Am. Meteorol. Soc.*, *95*(12), 1897–1908, doi:10.1175/BAMS-D-12-00243.1.

Drushka, K., J. Sprintall, and S. T. Gille (2014), Subseasonal variations in salinity and barrier-layer thickness in the eastern equatorial Indian Ocean, *J. Geophys. Res. Ocean.*, *119*(2), 805–823, doi:10.1002/2013JC009422.

Fairall, C. W., E. F. Bradley, J. E. Hare, A. A. Grachev, and J. B. Edson (2003), Bulk parameterization of air-sea fluxes: Updates and verification for the COARE algorithm, *J. Clim.*, *16*(4), 571–591, doi:10.1175/1520-0442(2003)016<0571:BPOASF>2.0.CO;2.

Girishkumar, M. S., M. Ravichandran, M. J. McPhaden, and R. R. Rao (2011), Intraseasonal variability in barrier layer thickness in the south central Bay of Bengal, *J. Geophys. Res.*, *116*(C3), C03009, doi:10.1029/2010JC006657.

Girishkumar, M. S., M. Ravichandran, and M. J. McPhaden (2013), Temperature inversions and their influence on the mixed layer heat budget during the winters of 2006-2007 and 2007-2008 in the Bay of Bengal, *J. Geophys. Res. Ocean.*, *118*(5), 2426–2437, doi:10.1002/jgrc.20192.

Halkides, D. J., L. E. Lucas, D. E. Waliser, T. Lee, and R. Murtugudde (2011), Mechanisms controlling mixed-layer temperature variability in the eastern tropical Pacific on the intraseasonal timescale, *Geophys. Res. Lett.*, *38*(17), doi:10.1029/2011GL048545.

Kurian, J., and P. N. Vinayachandran (2006), Formation mechanisms of temperature inversions in the southeastern Arabian Sea, *Geophys. Res. Lett.*, *33*(17), L17611, doi:10.1029/2006GL027280.

Lukas, R., and E. Lindstrom (1991), The mixed layer of the western equatorial Pacific Ocean, *J. Geophys. Res.*, *96*, 3343–3357, doi:10.1029/90JC01951.

- Maes, C., and T. J. O’Kane (2014), Seasonal variations of the upper ocean salinity stratification in the Tropics, *J. Geophys. Res. Ocean.*, *119*, 1706–1722, doi:10.1002/2013JC009366.
- Mignot, J., C. de B. Montégut, A. Lazar, and S. Cravatte (2007), Control of salinity on the mixed layer depth in the world ocean: 2. Tropical areas, *J. Geophys. Res.*, *112*(C10), C10010, doi:10.1029/2006JC003954.
- Mignot, J., A. Lazar, and M. Lacarra (2012), On the formation of barrier layers and associated vertical temperature inversions: A focus on the northwestern tropical Atlantic, *J. Geophys. Res.*, *117*(C2), C20210, doi:10.1029/2011JC007435.
- Monterey, G., and S. Levitus (1997), Seasonal Variability of Mixed Layer Depth for the World Ocean, *NOAA Atlas NESDIS 14*, U. S. Gov. Print. Off., Washington, D. C.
- Morel, A., and D. Antoine (1994), Heating rate within the upper ocean in relation to its bio-optical state, *J. Phys. Oceanogr.*, *24*, 1652–1665, doi:10.1175/1520-0485(1994)024<1652:HRWTUO>2.0.CO;2.
- Neetu, S., M. Lengaigne, E. M. Vincent, J. Vialard, G. Madec, G. Samson, M. R. Ramesh Kumar, and F. Durand (2012), Influence of upper-ocean stratification on tropical cyclone-induced surface cooling in the Bay of Bengal, *J. Geophys. Res.*, *117*(C12), C12020, doi:10.1029/2012JC008433.
- Praveen Kumar, B., J. Vialard, M. Lengaigne, V. S. N. Murty, and M. J. McPhaden (2011), TropFlux: air-sea fluxes for the global tropical oceans—description and evaluation, *Clim. Dyn.*, *38*(7-8), 1521–1543, doi:10.1007/s00382-011-1115-0.
- Rao, R. R., and R. Sivakumar (2000), Seasonal variability of near-surface thermal structure and heat budget of the mixed layer of the tropical Indian Ocean from a new global ocean temperature climatology, *J. Geophys. Res.*, *105*(C1), 995–1015, doi:10.1029/1999JC900220.
- Rao, R. R., and R. Sivakumar (2003), Seasonal variability of sea surface salinity and salt budget of the mixed layer of the north Indian Ocean, *J. Geophys. Res.*, *108*(C1), 9–1 – 9–14, doi:10.1029/2001JC000907.
- Roxy, M., and Y. Tanimoto (2007), Role of SST over the Indian Ocean in Influencing the Intraseasonal Variability of the Indian Summer Monsoon, *J. Meteorol. Soc. Japan*, *85*(3), 349–358, doi:10.2151/jmsj.85.349.
- Shankar, D., V. V. Gopalakrishna, S. S. C. Shenoi, F. Durand, S. R. Shetye, C. K. Rajan, Z. Johnson, N. A. And, and G. S. Michael (2004), Observational evidence for westward propagation of temperature inversions in the southeastern Arabian Sea, *Geophys. Res. Lett.*, *31*(8), L08305, doi:10.1029/2004GL019652.
- Shenoi, S. S. C., D. Shankar, and S. R. Shetye (2002), Differences in heat budgets of the near-surface Arabian Sea and Bay of Bengal : Implications for the summer monsoon, *J. Geophys. Res.*, *107*(C6), 1–14, doi:10.1029/2000JC000679.
- Sweeney, C., A. Gnanadesikan, S. M. Griffies, M. J. Harrison, A. J. Rosati, and B. L. Samuels (2005), Impacts of Shortwave Penetration Depth on Large-Scale Ocean Circulation and Heat Transport, *J. Phys. Oceanogr.*, *35*(6), 1103–1119, doi:10.1175/JPO2740.1.
- Thadathil, P., and A. K. Gosh (1992), Surface layer temperature inversion in the Arabian Sea during winter, *J. Oceanogr.*, *48*(3), 293–304, doi:10.1007/BF02233989.

Thadathil, P., V. V Gopalakrishna, P. M. Muraleedharan, G. V Reddy, N. Araligidad, and S. Shenoy (2002), Surface layer temperature inversion in the Bay of Bengal, *Deep -Sea Res. Part I*, 49(10), 1801–1818, doi:10.1016/S0967-0637(02)00044-4.

Thadathil, P., P. M. Muraleedharan, R. R. Rao, Y. K. Somayajulu, G. V. Reddy, and C. Revichandran (2007), Observed seasonal variability of barrier layer in the Bay of Bengal, *J. Geophys. Res.*, 112(C2), C02009, doi:10.1029/2006JC003651.

Thompson, B., C. Gnanaseelan, and P. S. Salvekar (2006), Seasonal evolution of temperature inversions in the north Indian Ocean, *Curr. Sci.*, 90(5), 697.

Vialard, J., P. Terray, J.-P. Duvel, R. S. Nanjundiah, S. S. C. Shenoi, and D. Shankar (2011), Factors controlling January–April rainfall over southern India and Sri Lanka, *Clim. Dyn.*, 37(3-4), 493–507, doi:10.1007/s00382-010-0970-4.

Figure captions

Figure 1: (a) Trajectory (of the Argo float (ID No. 5903744) during 02 January - 22 March, 2013. Green squares indicate the positions of the four RAMA buoys located in the BoB. (b) Vertical profile of salinity (blue) and temperature (red) from Argo float on 27 January 2013 and illustration of SLTI and the associated parameters: ΔT , ΔS , LT and T_{\max} (see text for definitions). The blue shaded region marks SLTI. Time evolution of three hourly (c) **temperature** and (d) salinity profiles from the Argo float during 02 January – 22 March, 2013.

Figure 2: Time evolution of temperature (left panels) and salinity (right panels) vertical profiles during winter 2012-2013 for the RAMA buoys located along 90°E at (top) 15°N , (middle top) 12°N , (middle bottom) 8°N , and (bottom) 4°N . The dashed and solid lines show MLD and ILD, respectively. Filled circles indicate the presence of temperature inversion with colours indicating the amplitudes of ΔT and are placed at the middle of SLTI.

Figure 3: Seasonal variability of mean ΔT , LT and occurrence frequency at the four RAMA buoys located in the BoB. Seasonal variations are derived by averaging the parameters available over a period of 7 years (2006-2014).

Figure 4: Same as in Figure 3, but for the buoy at 15°N for seven winters during 2007-2014.

Figure 5: Time evolution of (a) ΔT and (b) LT during December-January-February period of the seven winters over 2007-2014. The red horizontal bars indicate the mean value of seasonal anomalies (by removing the seasonal variations) during December – February for each year and are considered as the interannual component. Intraseasonal fluctuations are defined as the deviation from the interannual anomalies after removing the seasonal cycle (black dots minus seasonal cycle minus the red bars). The standard deviation of the intraseasonal and interannual ΔT and LT variations over the entire period are provided on the respective panels.

Figure 6: Scatter plot of (a) ILD vs. LT and (b) ΔT vs. LT. The correlation coefficients (r) are indicated in the respective panels, with those significant at 95% confidence level are bold faced.

Figure 7: Normalized distribution (in percentage) of SSS during inversion (red) and non-inversion (blue) cases. Profiles with $\Delta T > 0.1^{\circ}\text{C}$ only are treated as having temperature inversion.

Figure 8: Scatter plots of ΔT vs. (a) ΔS , (b) SSS, (c) SST seasonal anomalies and (d) T_{\max} seasonal anomalies. The correlations between each pair of variables are indicated on the respective panels, with those significant at 95% confidence level are bold faced.

Figure 9: Mixed layer heat budget analysis. Time series from (a) October 2008 to May 2009 (b) October 2009 to May 2010 and (c) October 2012 to May 2013 of SST tendency (black) and the contributing terms: atmospheric forcing (red), horizontal advection (blue) and remainder (yellow) terms. Thick portions of the lines indicate the presence of inversion during those periods.

Figure 10: (Upper panels) Scatter plots of SST tendency against (a) atmospheric forcing term, (b) horizontal advection and (c) remainder. (Bottom panels) Scatter plots of net heat flux against (d) latent heat flux, (e) shortwave flux and (f) penetrative shortwave flux below the mixed layer. The correlations (r) and regression coefficients (reg) are provided within each panel. The correlations significant at 95% confidence level are bold faced.

Figure 11: Weekly maps of seasonal (left panels) SST from AVHRR and (right panels) SSS from AQUARIS, superimposed with surface currents (geostrophic + Ekman) from OSCAR current. The black line in the left panel shows the demarcation of cold and warm anomalies. RAMA buoy location (15°N , 90°E) is marked by a black star.

Figure 12: (a) Scatter plot of remainder term against ΔT during inversion period. (b) Averaged amplitude of the remainder term for non-inversion cases (blue bar) and inversion cases as a function of ΔT (red bars). The correlation (r) significant at 95% level is bold faced.

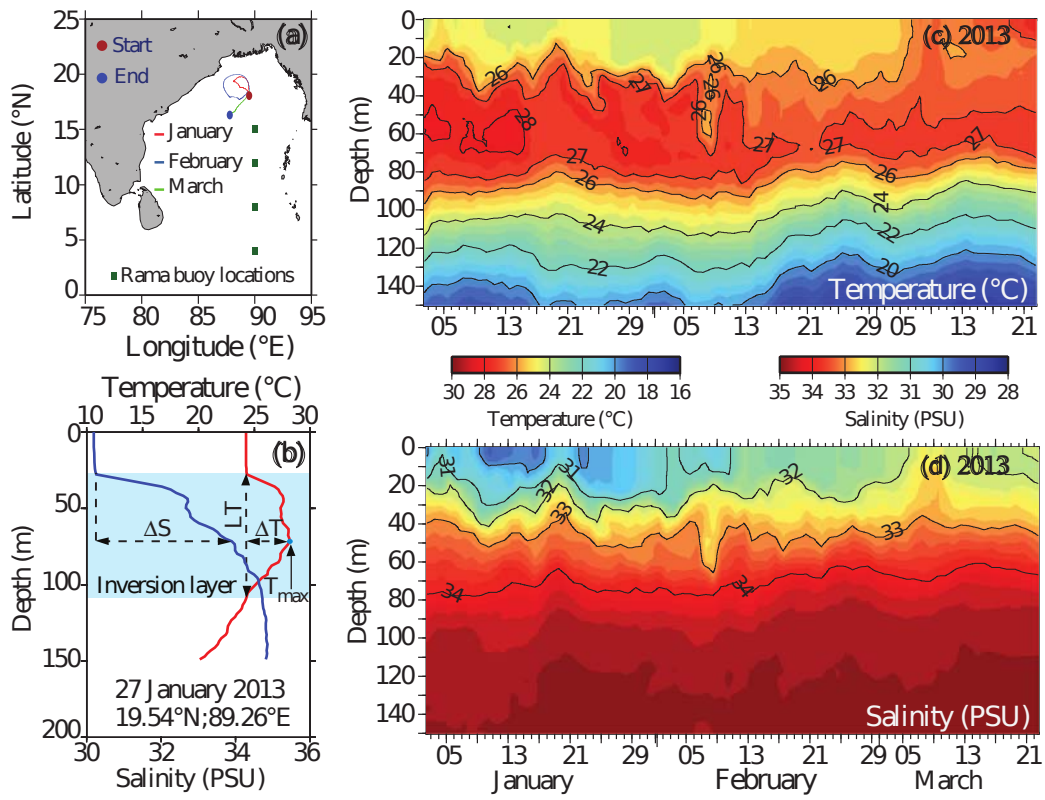


Figure 1

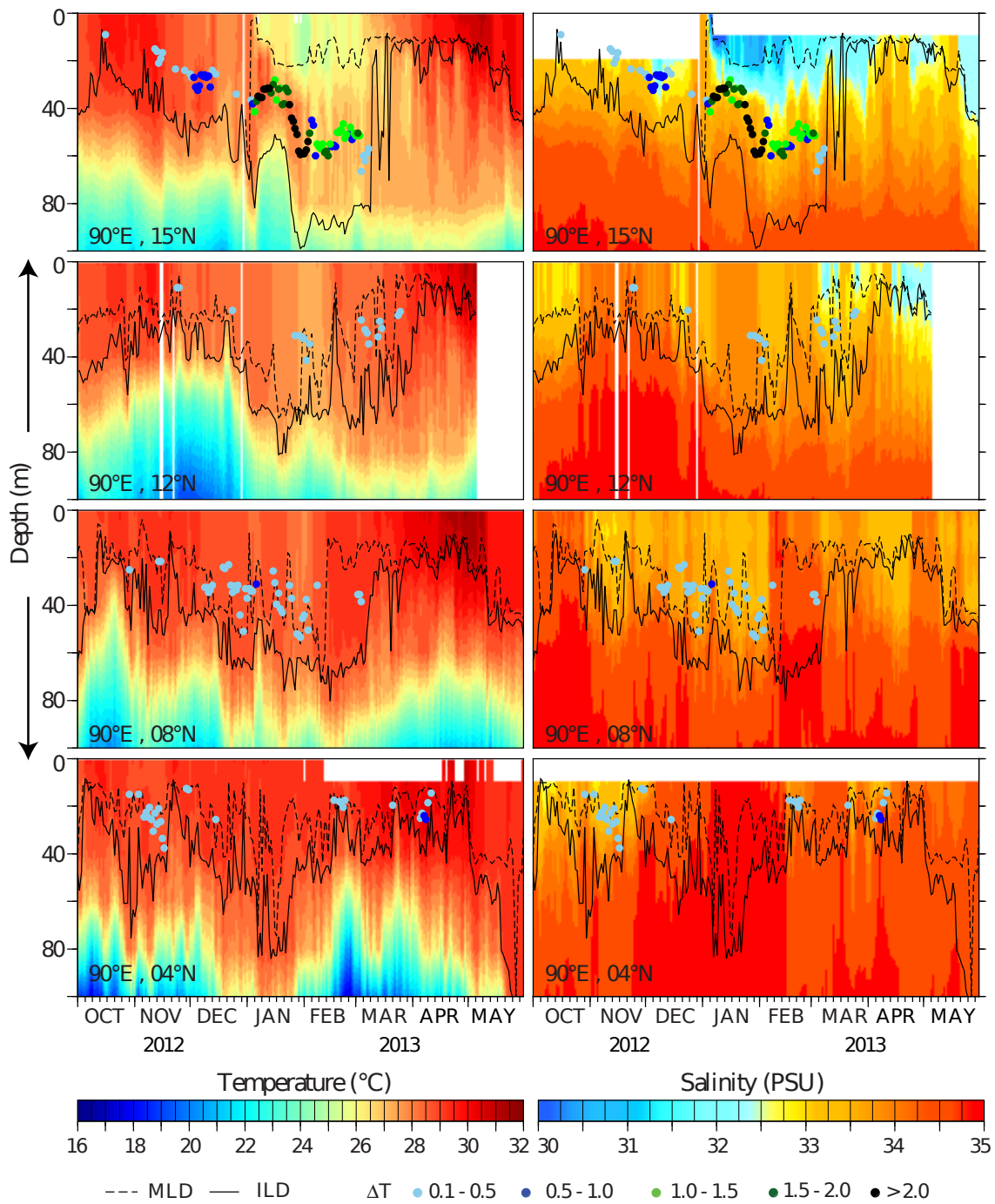


Figure 2

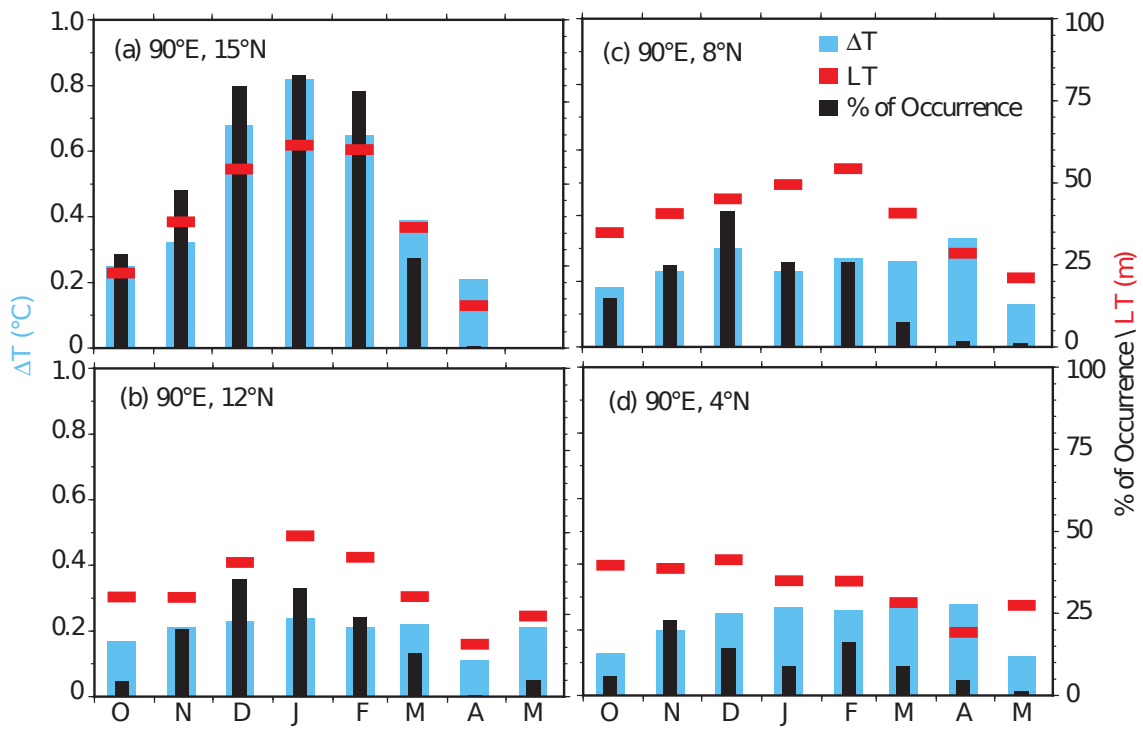


Figure 3

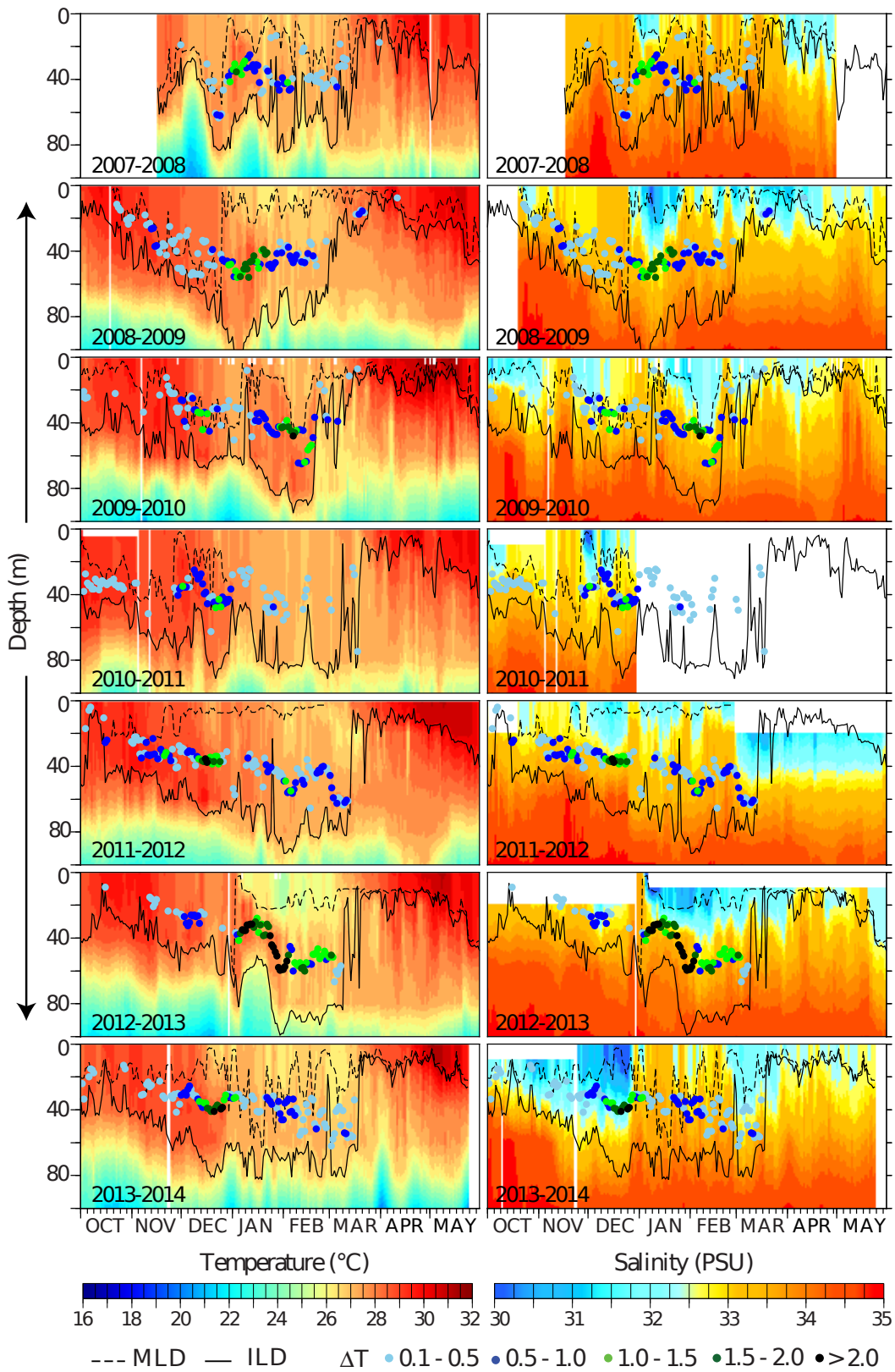


Figure 4

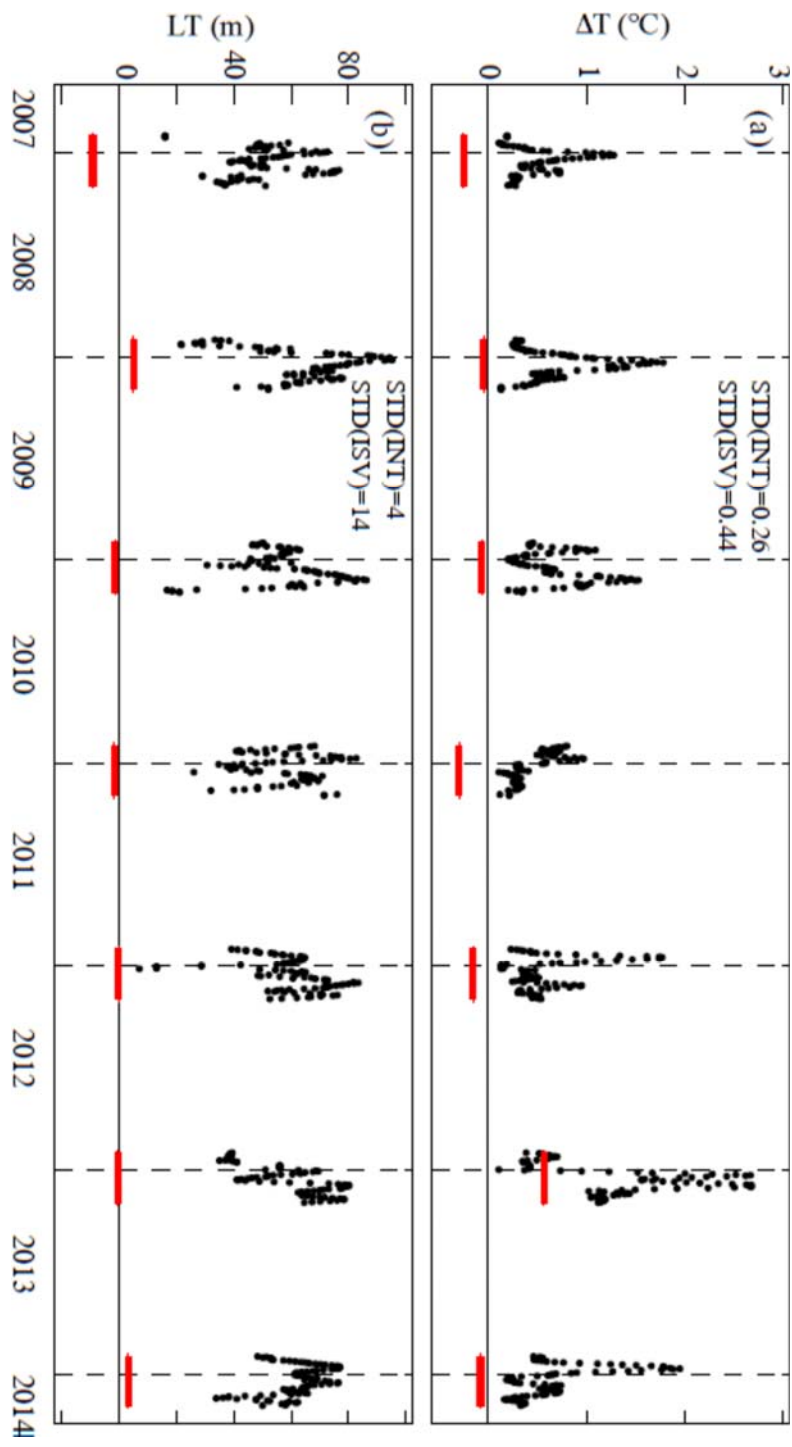


Figure 5

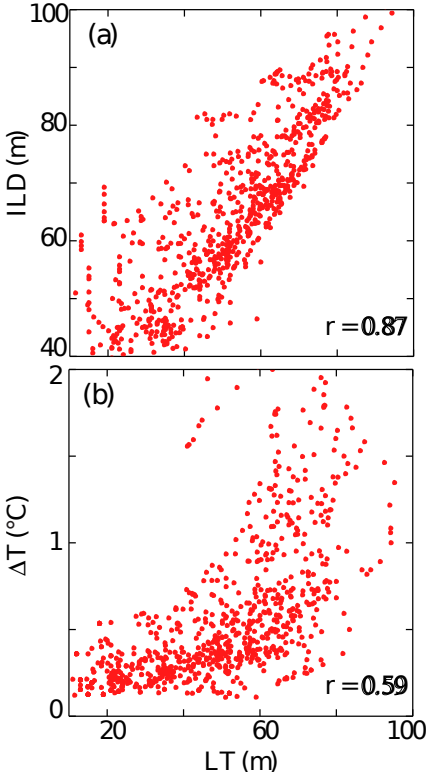


Figure 6

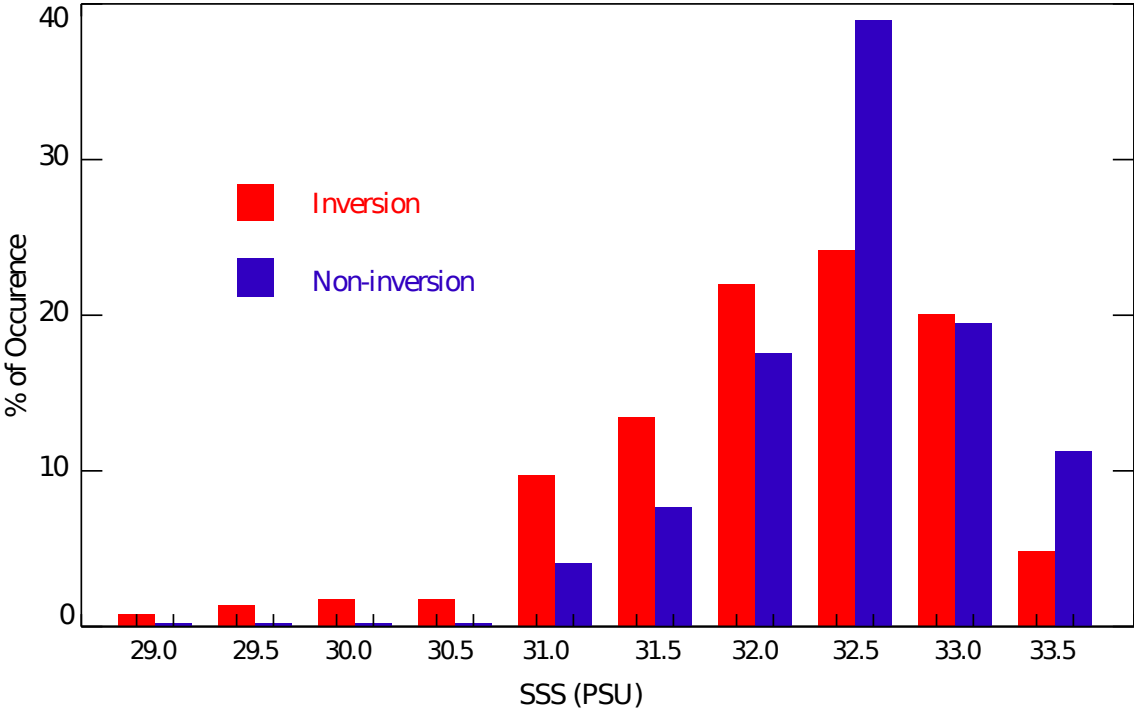


Figure 7

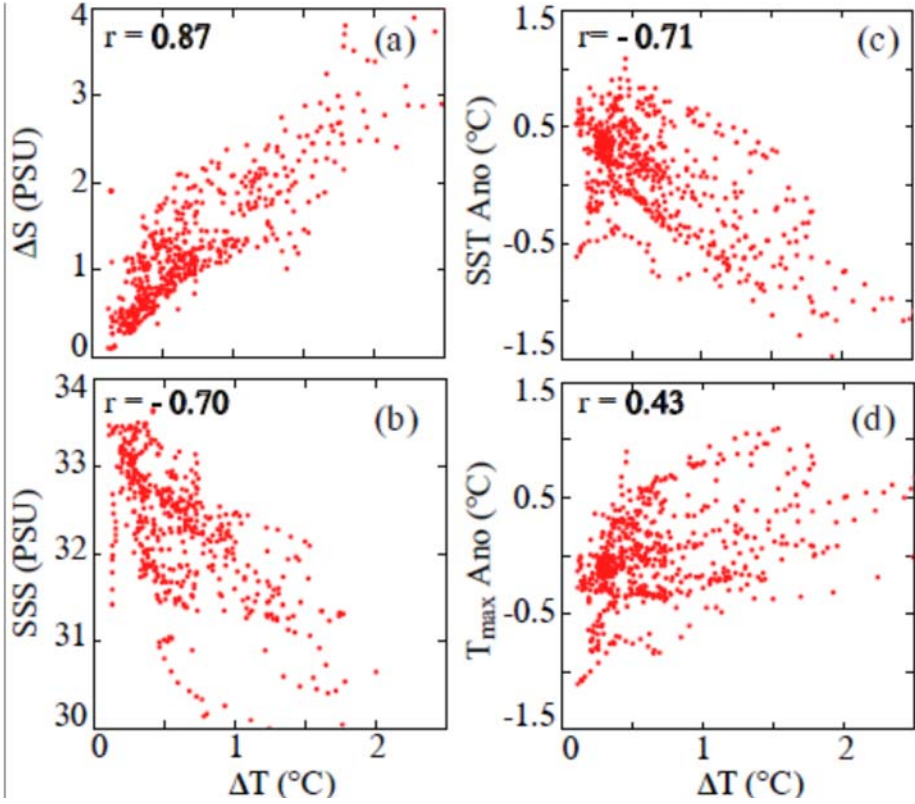


Figure 8

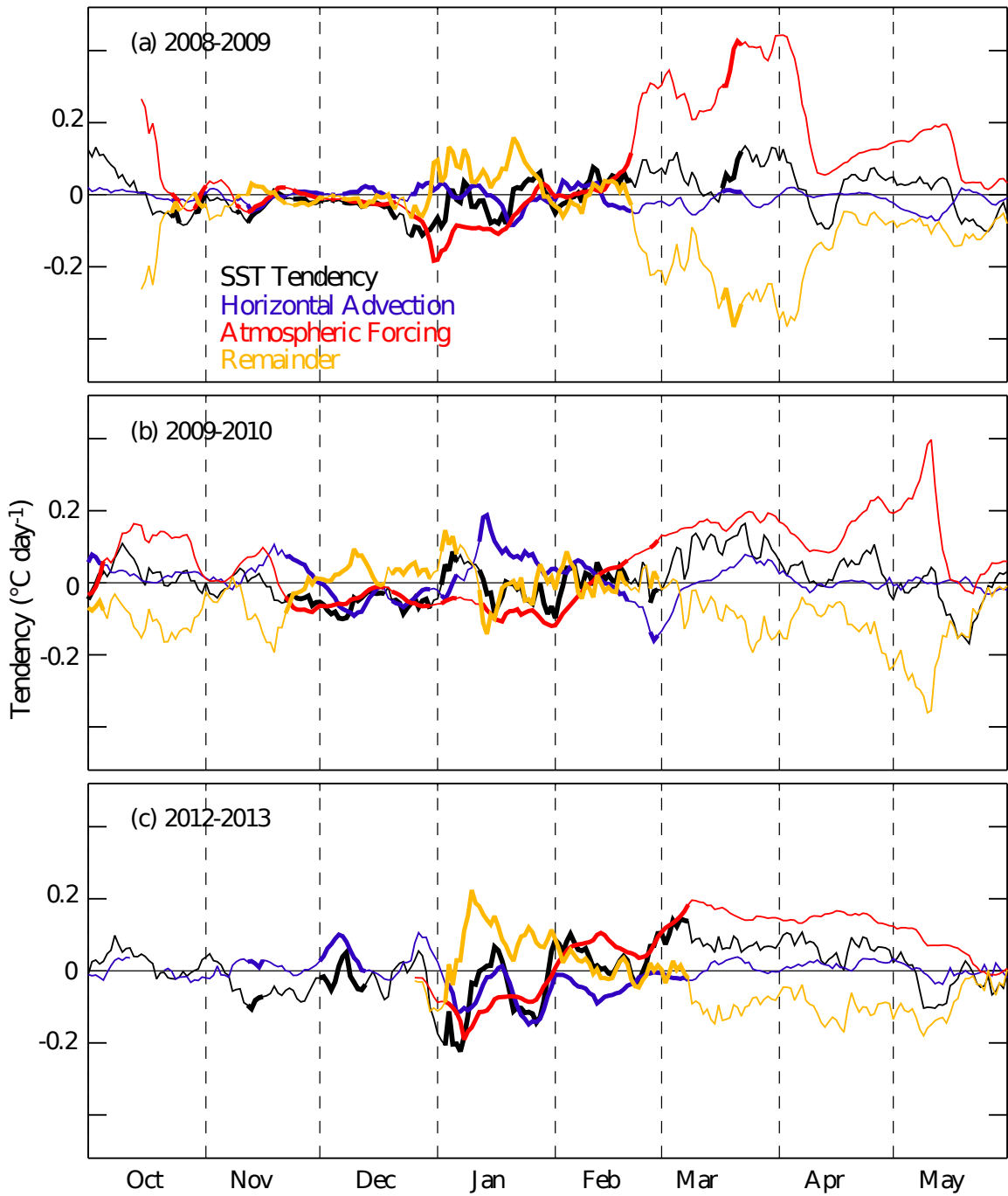


Figure 9

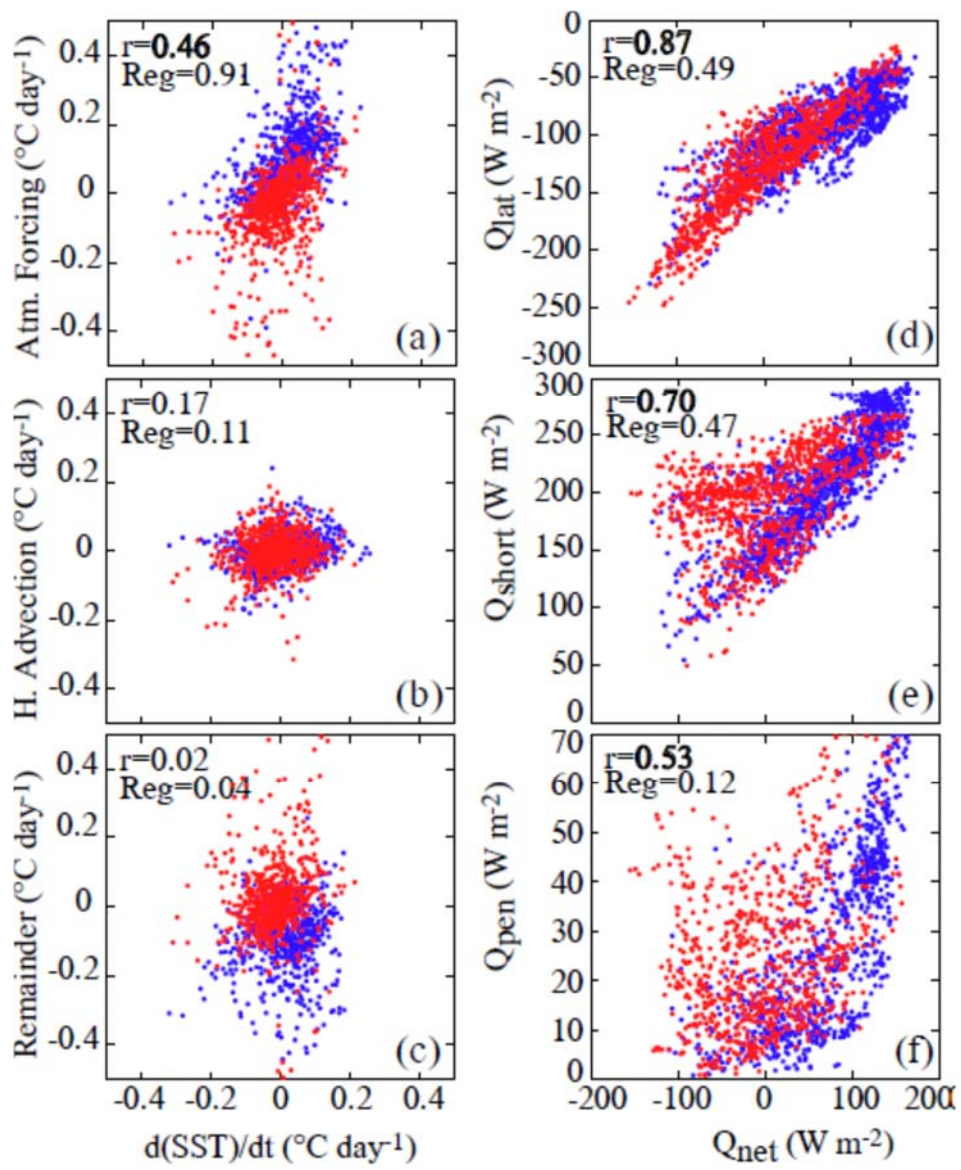


Figure 10

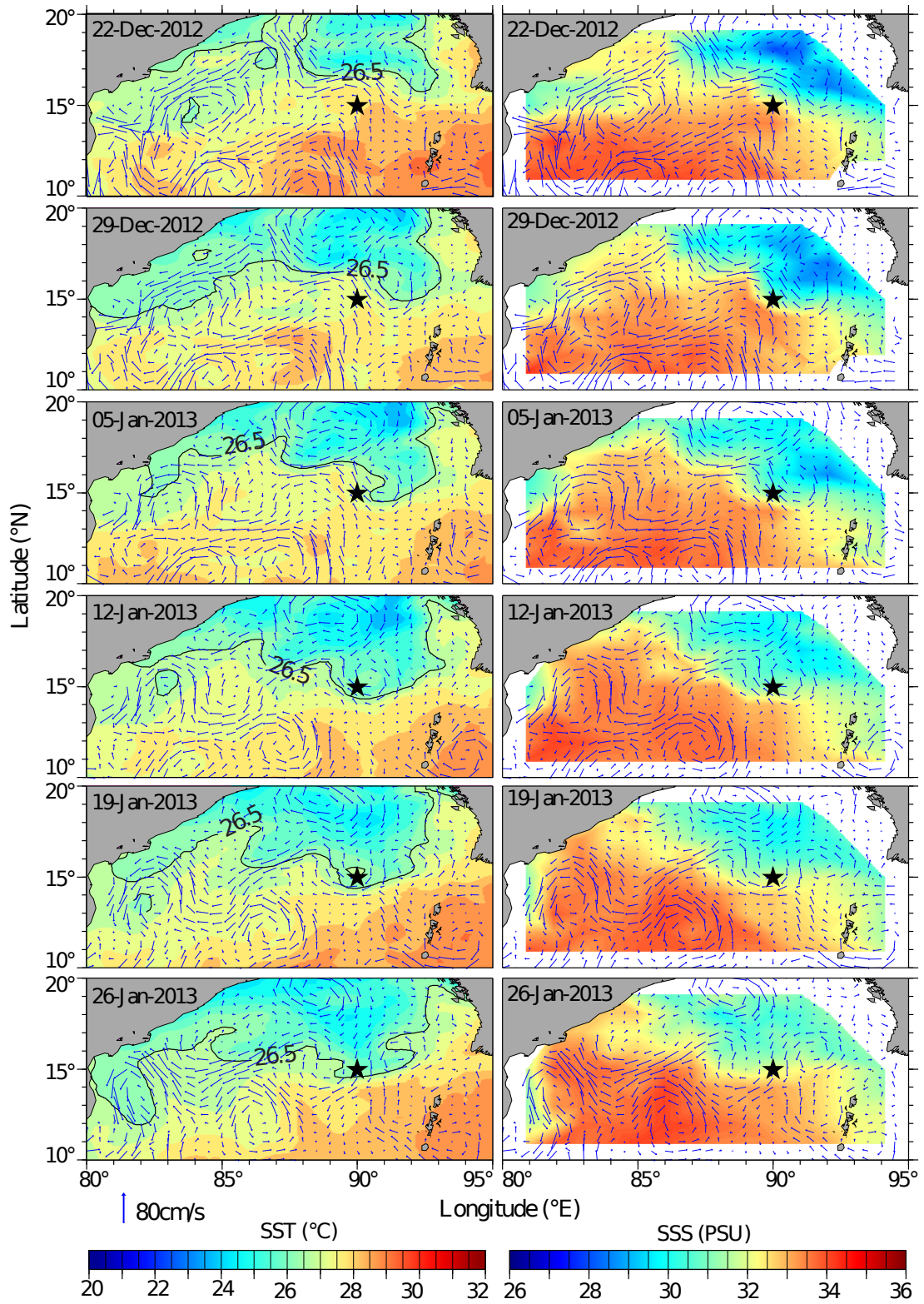


Figure 11

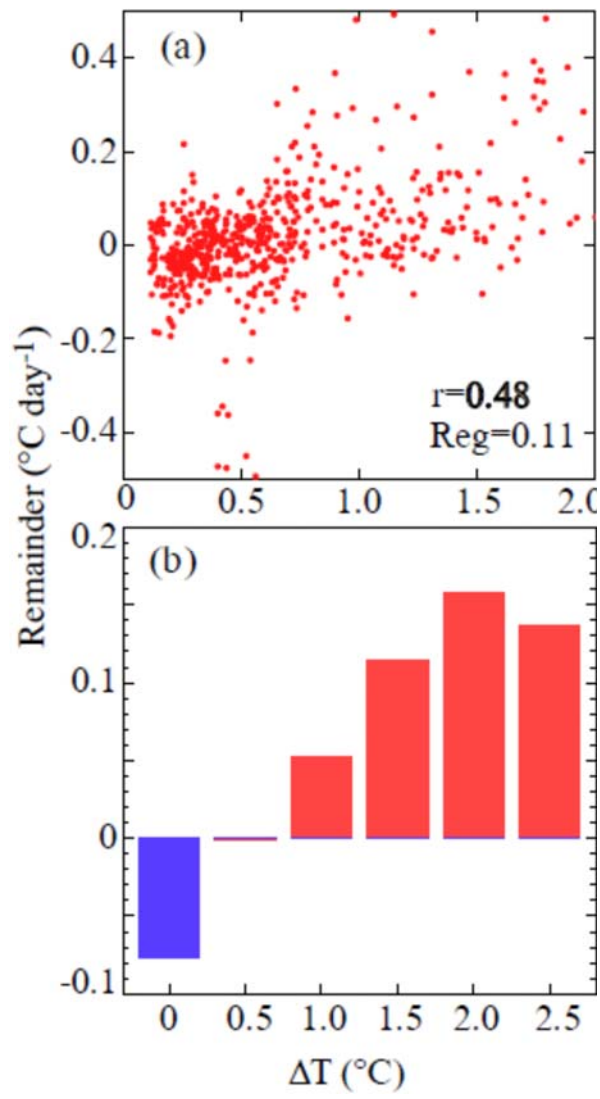


Figure 12